




Short Communication

Supercapacitive performance of C-axis preferentially oriented TiO₂ nanotube arrays decorated with MnO₂ nanoparticles

Liuji Wang¹  · Jie Yang¹ · Zhihua Ma¹ · Pengfa Li¹

© Springer Nature Switzerland AG 2019

Abstract

A novel composite supercapacitor electrode material, MnO₂ @ (004) preferred oriented TiO₂ nanotube arrays (p-MTNAs) had been synthesized via anodizing method and hydrothermal deposition. The experimental results showed that the introduction of p-TNAs to MnO₂ could improve the electrochemical properties compared to the MnO₂ @ random crystallography oriented TiO₂ nanotube arrays (r-MTNAs), the reason was that the p-TNAs increased the electric conductivity for faster ion transport. The highest specific capacitance of p-MTNAs electrode could reach 190.6 F/g at the current density of 1 A/g. Moreover, p-MTNAs showed superior cycling stability, remaining 88% of its initial capacitance after 2000 cycles.

Keywords Nanotube arrays · Preferred oriented · Electric conductivity · Composite supercapacitor

1 Introduction

In recent years, great attentions had been paid on supercapacitors (SCs) because of its own intrinsic characteristics including natural abundance, low cost and environmental friendliness etc. [1, 2]. The pseudocapacitors were mainly made of transition metals oxides such as manganese dioxide (MnO₂) [3], ferric oxide (Fe₂O₃) [4], cobaltic oxide (Co₃O₄) [5], vanadic oxide (V₂O₅) [6] and cuprous oxide (Cu₂O) [7]. Among above-mentioned oxygenate, MnO₂ was among the most promising materials in supercapacitor system [8]. The capacitance of actual MnO₂ was rarely achieving the theoretical specific capacitance owing to inherent low electronic conductivity and limited surface of thick layers. So there were two effective methods to increase performance: (1) MnO₂ nanoparticles were synthesized to increase the surface area, while adding a thin layer in electrochemical reactive redox process. (2) Conductive materials were used to improve electrical conductivity [9].

Recently, highly ordered TiO₂ nanotube arrays [10, 11] (TNAs) had stimulated more and more interests in the electrode materials for supercapacitor, but the poor electric conductivity of TNAs results in a relatively low specific capacitance. There were some strategies to improve the capacitance properties including the introduction of oxygen vacancies [12], fabricated H-ion doping TNAs [13]. Compared with transition metal oxides, the capacitance of TNAs was still too low. So the important method to improve capacitance of TNAs was introduced metal oxides deposited on the surface of tubes to improve capacitance [14–16].

In this paper, the p-TNAs could provide high surface area and improve considerably electronic conductivity [17, 18]. The p-TNAs could be used as a suitable carrier for MnO₂ nanoparticles to form composite electrode materials structures. The MnO₂/p-TNAs electrodes contained advantages of combining p-TNAs and MnO₂ nanoparticles and exhibited high electrochemical performance and cycling stability.

Electronic supplementary material The online version of this article (<https://doi.org/10.1007/s42452-019-0580-7>) contains supplementary material, which is available to authorized users.

✉ Zhihua Ma, 86547309@qq.com; ✉ Pengfa Li, lipfyouxiang@163.com | ¹College of Chemistry and Chemical Engineering, Xinxiang University, Xinxiang 453003, People's Republic of China.



SN Applied Sciences (2019) 1:563 | <https://doi.org/10.1007/s42452-019-0580-7>

Received: 19 March 2019 / Accepted: 8 May 2019 / Published online: 14 May 2019

SN Applied Sciences
A SPRINGER NATURE journal

2 Experimental

2.1 Materials preparation

The p-TNAs were fabricated via the potentiostatic anodization method [17]. In brief, the p-TNAs were fabricated at 50 V in glycol electrolyte which contained 0.25 wt% NH_4F and 2 wt% H_2O for 2 h. The r-TNAs were fabricated at 60 V in glycol electrolyte which contained 0.25 wt% NH_4F and 2 wt% H_2O for 2 h. The crystallization process of p-TNAs and r-TNAs was obtained by annealing at Ar air atmosphere with a ramping rate of 5°C min^{-1} up to 450°C maintained 3 h. After annealing process, the p-TNAs and r-TNAs were put into a Teflonlined stainless steel autoclave containing 0.02 M KMnO_4 . The autoclave was then maintained at 150°C for 5 h to donate as p-MTNAs and r-MTNAs.

2.2 Material characterization

Field emission scanning electron microscopy (FE-SEM) used in the present this work was a FEI Quanta 250 FEG. High-resolution transmission electron microscopy (HR-TEM) was carried out FEI Talos F 200X. X-ray diffraction (XRD) patterns were obtained with a Bruker D8 diffractometer using Cu K α radiation ($\lambda = 1.5418 \text{ \AA}$, 40 kV, 40 mA). X-ray photoelectron spectrum (XPS) was performed on Thermo Fisher Escalab Xi+.

2.3 Electrochemical measurements

All electrochemical properties were investigated by cyclic voltammetry (CV) and galvanostatic charge–discharge (GCD) measurements on an electrochemical workstation (IVIUM Ivium Stat.h, Netherlands) at room temperature. In a traditional three-electrode cell, the p-MTNAs was used as working electrodes, and an Ag/AgCl (3 M KCl) and a Pt poil were used as reference and counter electrodes, 1 M Na_2SO_4 solution as the electrolyte respectively. The cycling stability was measured by GCD tests up to 2000 cycles at a current density of 1 A/g.

3 Results and discussion

Figure 1a showed a highly ordered nanotubes of the p-TNAs with a diameter of $90 \pm 2 \text{ nm}$ and wall thickness of $15 \pm 1 \text{ nm}$, respectively. The morphology of p-MTNAs (Fig. 1b) had not unchanged compared with p-TNAs, so it could be seen from the above results that the deposition of MnO_2 nanoparticles on TNAs surface was very uniform. The TEM and HR-TEM were used for further morphology

and structure characterization. HR-TEM images of the p-MTNAs nanotube wall were displayed in Fig. 1c, d, which indicated that the lattice fringes and the mouth of nanotubes in parallel. Further analysis showed that the interplanar spacing was 0.236 nm which was in accord with the (001) plane of the anatase phase [17].

Figure 2a displayed the XRD patterns of Ti foils, the p-MTNAs and r-MTNAs. The XRD pattern of Ti foils indicated the polycrystalline characteristic and the peak [18] at $2\theta = 38.5, 40.3, 50.2$ and 70.8° of the Ti foils, which correspond to the (002), (101), (102) and (103) planes of hexagonal titanium (JCPDS no. 44-1294). The r-MTNAs showed the diffraction peaks at $2\theta = 25.4, 38.0$ and 48.2° , which correspond to the (101), (004), and (200) planes of the TiO_2 anatase phase (JCPDS card no.21-1272). In addition, it was noteworthy that the p-MTNAs (Fig. 2a) showed the (004) preferred orientation and the r-MTNAs (Fig. 2a) was polycrystalline. Because MnO_2 nanoparticles were relatively few, there was no diffraction peak of MnO_2 nanoparticles in the XRD patterns. Figure 2b showed remarkable O1s core level XPS spectra of p-MTNAs. The p-MTNAs samples exhibited the peak of 529.6 eV which corresponds to the $\text{Ti}^{4+}\text{-O}$ bond. The decomposition of the O1s spectrum of p-MTNAs revealed three additional peaks centered at 530.3, 531.2 and 532.1 eV which should be attributed to $\text{Mn}^{4+}\text{-O}$, $\text{Ti}^{3+}\text{-O}$ and Ti-OH bonds respectively [20]. In Fig. 2c, the Ti 2p XPS spectra of the p-MTNAs in which two broad peaks centered were found at about 458.1 and 463.9 eV, the peaks of p-MTNAs showed a negative shift comparison to the TNAs [11]. In Fig. 2d, the XPS spectra of p-MTNAs showed the peaks of Mn 2p $_{3/2}$ and Mn 2p $_{1/2}$ centered at 642.1 and 653.9 eV, respectively [19].

Figure 3 showed the CV curves of the p-MTNAs and r-MTNAs at the scan rates of 100 mV s^{-1} in 1 M Na_2SO_4 aqueous electrolyte. At 100 mV s^{-1} , the shapes of all curves of the p-MTNAs and r-MTNAs were quasi rectangular (not perfectly rectangular owing to polarization resistance [20]) which indicated the desired capacitive behavior and high rate capability. The areal capacitance of the as-prepared samples were calculated from the CV curves using the following equation [21–23]: $C_A = \frac{I\Delta t}{A\Delta V}$. The p-MTNAs showed higher specific capacitance (253 F/g) than the capacitance of r-MTNAs (93 F/g) at 5 mV s^{-1} . The experimental results showed the existence of Ti^{3+} and oxygen vacancies led to ultrahigh conductivity [17], which was propitious to the charge transfer of the ions and electrons between active MnO_2 materials and p-TNAs. As showed in Fig. 3b, along with the scanning rate increasing, the decreased C_g was ascribed to the reduction of the active reaction sites at high scan rate.

The GCD curves of the p-MTNAs and r-MTNAs were shown in Fig. 3c. It could be seen that all the discharge and charge curves were not perfect straight line, not perfectly

Fig. 1 FESEM images of the **a** p-TNAs and **b** p-MTNAs; TEM and HR-TEM images of the **(c)** and **d** p-MTNAs

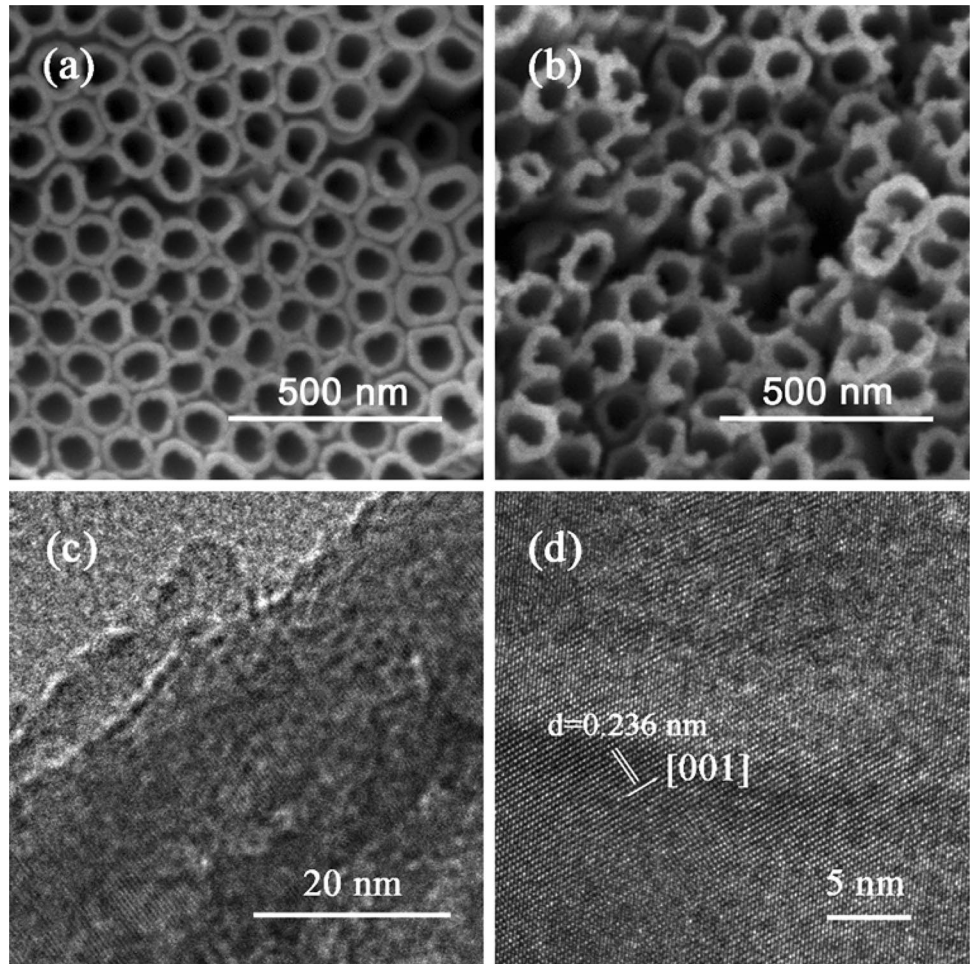


Fig. 2 **a** XRD patterns of Ti foils, r-MTNAs and p-MTNAs; **b** XPS peaks of O 1s of p-MTNAs; **c** XPS peaks of Ti 2p of p-MTNAs; **d** XPS peaks of Mn 2p of p-MTNAs

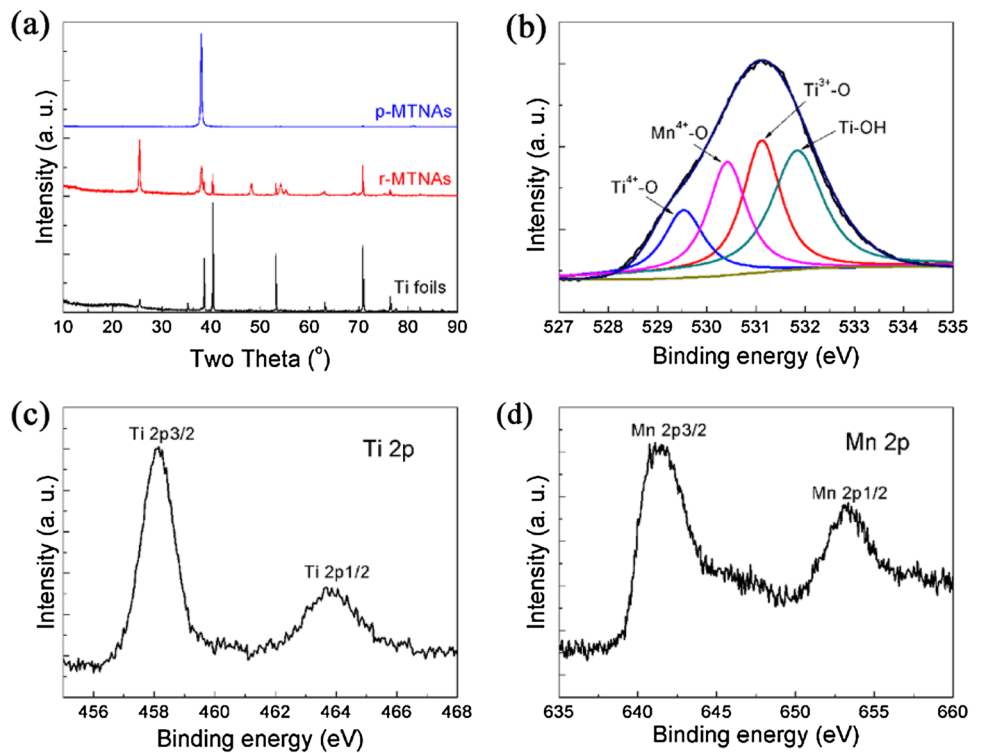
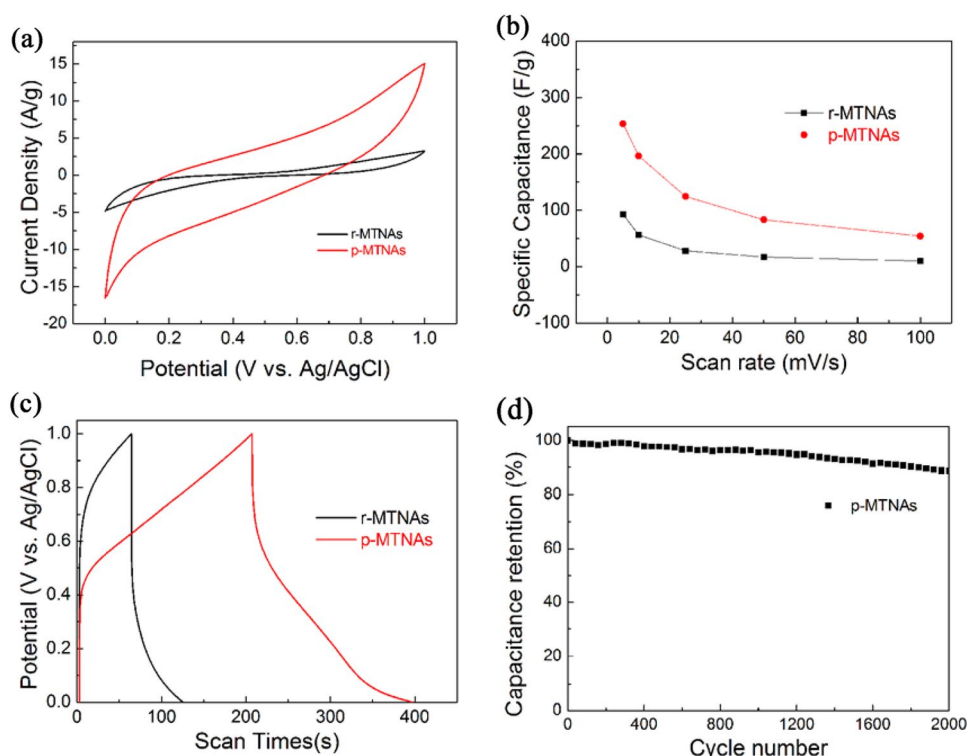


Fig. 3 **a** CV curves of Samples at the scan rate of 100 mV/s, **b** Gravimetric capacitance of samples I-V taken from the CV measurement at different scan rates, **c** Discharge and charge curves of p-MTNAs and r-MTNAs at the current density of 1 A/g, **d** The galvanostatic cycling curve of p-MTNAs electrode at 1 A/g



symmetrical and the obvious iR drops. The above results indicated that these p-MTNAs electrodes showed Faradic capacitive performance [24] and the intrinsically poor conductivity of p-TNAs and MnO_2 nanoparticles. Figure 3c showed that the charge–discharge time of the p-MTNAs electrodes was significantly enhanced than the r-MTNAs electrodes at the current density of 1 A/g, indicating that the p-MTNAs electrodes possessed the higher specific capacitance. This result was well consistent with the above results of CV tests.

The long-term cycle stability of p-MTNAs electrode was also assessed in this paper by the representative galvanostatic cycling at a current density of 1 A/g for 2000 cycles (Fig. 3d). The results indicated that the p-MTNAs electrode showed 88% initial capacitance retention after 2000 cycles. It implied that p-MTNAs electrode revealed little capacitance losses even after 2000 cycles.

4 Conclusion

The composite structure MnO_2/p -MTNAs was fabricated on metal Ti foils by the anodizing method and hydrothermal method. The improvement on specific capacitances was turned out to be owing to the synergism of the existence of p-TNAs. The existence of oxygen vacancies improved the inferior conductivity of TiO_2 nanotube arrays. The deposition of MnO_2 nanoparticles carried out

fast and reversible faradaic redox reactions at the electrode–electrolyte interfaces. The notable long-term cycle stability could also be obtained due to the excellent electrical conductivity.

Acknowledgements This work was financially supported by the National Natural Science Foundation of China (NSFC 51701173), the National Natural Science Foundation of China (NSFC 51871190) and the Key Research Project of Chinese Universities (18A530004).

Compliance with ethical standards

Conflicts of interest There are no conflicts to declare.

References

- Zhang D, Miao M, Niu H, Wei Zh (2014) Core-spun carbon nanotube yarn supercapacitors for wearable electronic textiles. *ACS Nano* 8(5):4571–4579
- Shao Y, Kady M, Sun J, Li Y, Zhang Q, Zhu M, Wang H, Dunn B, Kaner R (2018) Design and mechanisms of asymmetric supercapacitors. *Chem Rev* 118(18):9233–9280
- Tanggarnjanavalukul C, Phattharasupakun N, Kongpatpanichb K, Sawangphruk M (2017) Charge storage performances and mechanisms of MnO_2 nanospheres, nanorods, nanotubes and nanosheets. *Nanoscale* 9:13630–13639
- Li J, Wang N, Deng J, Qian W, Chu W (2018) Flexible metal-templated fabrication of mesoporous onion-like carbon and $Fe_2O_3@N$ -doped carbon foam for electrochemical energy storage. *J Mater Chem A* 6:13012–13020

- Hao J, Peng Sh, Li H, Dang Sh, Qin T, Wen Y, Huang J, Ma F, Gao D, Li F, Cao G (2018) A low crystallinity oxygen-vacancy-rich Co_3O_4 cathode for high-performance flexible asymmetric supercapacitors. *J Mater Chem A* 6:16094–16100
- Yang J, Lan T, Liu J, Song Y, Wei M (2013) Supercapacitor electrode of hollow spherical V_2O_5 with a high pseudocapacitance in aqueous solution. *Electrochim Acta* 105:489–495
- Guan H, Cai P, Zhang X, Zhang Y, Chen G, Dong Ch (2018) Cu_2O templating strategy for the synthesis of octahedral $\text{Cu}_2\text{O}@\text{Mn}(\text{OH})_2$ core-shell hierarchical structures with a superior performance supercapacitor. *J Mater Chem A* 6:13668–13675
- Zhang Q, Zhang D, Miao Z, Zhang X, Chou Sh (2018) Research progress in MnO_2 -carbon based supercapacitor electrode materials. *Small* 14(24):1702883
- Maqbool Q, Singh C, Jash P, Paul A, Srivastava A (2017) Nano “Koosh balls” of mesoporous MnO_2 : improved supercapacitor performance through superior ion transport. *Chem Eur J* 23(17):4216–4226
- Wang B, Cao J, Dong Y, Liu F, Fu X, Ren Sh, Ma Sh, Liu Y (2018) An in situ electron donor consumption strategy for photoelectrochemical biosensing of proteins based on ternary $\text{Bi}_2\text{S}_3/\text{Ag}_2\text{S}/\text{TiO}_2$ NT arrays. *Chem Commun* 54:806–809
- Lu X, Wang G, Zhai T, Yu M, Gan J, Tong Y, Li Y (2012) Hydrogenated TiO_2 nanotube arrays for supercapacitors. *Nano Lett* 12(3):1690–1696
- Zhou H, Zhang Y (2014) Electrochemically self-doped TiO_2 nanotube arrays for supercapacitors. *J Phys Chem C* 118(11):5626–5636
- Salari M, Konstantinov K, Liu H (2011) Enhancement of the capacitance in TiO_2 nanotubes through controlled introduction of oxygen vacancies. *J Mater Chem* 21:5128–5133
- Feng J, Xu H, Dong Y, Lu X, Tong Y, Li G (2017) Efficient hydrogen evolution electrocatalysis using cobalt nanotubes decorated with titanium dioxide. *Nanodots Angew Chem Int Ed* 56:2960–2964
- Feng J, Wu J, Tong Y, Li G (2018) Efficient hydrogen evolution on Cu nanodots-decorated Ni_3S_2 nanotubes by optimizing atomic hydrogen adsorption and desorption. *J Am Chem Soc* 140(2):610–617
- Feng J, Tong S, Tong Y, Li G (2018) Pt-like hydrogen evolution electrocatalysis on PANI/CoP hybrid nanowires by weakening the shackles of hydrogen ions on the surfaces of catalysts. *J Am Chem Soc* 140(15):5118–5126
- Pan D, Huang H, Wang X, Wang L, Liao H, Li Zh, Wu M (2014) C-axis preferentially oriented and fully activated TiO_2 nanotube arrays for lithium ion batteries and supercapacitors. *J Mater Chem A* 2:11454–11464
- Wang L, Wang Y, Yang Y, Wen X, Xiang H, Li Y (2015) Fabrication of different crystallographically oriented TiO_2 nanotube arrays used in dye-sensitized solar cells. *RSC Adv* 5:41120–41124
- Kim K, Park S (2012) Synthesis and high electrochemical performance of polyaniline/ MnO_2 -coated multi-walled carbon nanotube-based hybrid electrodes. *J Solid State Electrochem* 16(8):2751–2758
- Eustache E, Douard C, Retoux R, Lethien C, Brousse T (2015) MnO_2 Thin Films on 3D Scaffold: microsupercapacitor Electrodes Competing with “Bulk” Carbon Electrodes. *Adv Energy Mater* 5(18):1500680
- Shen B, Guo R, Lang J, Liu L, Liu L, Yan X (2016) A high-temperature flexible supercapacitor based on pseudocapacitive behavior of FeOOH in an ionic liquid electrolyte. *J Mater Chem A* 4:8316–8327
- Guo R, Chen J, Yang B, Liu L, Su L, Shen B, Yan X (2017) In-Plane Micro-Supercapacitors for an Integrated Device on One Piece of Paper. *Adv Funct Mater* 27(43):1702394
- Guo H, Liu L, Dou Q, Qin S, Zhu J, Chen J, Li Y, Li J, Yan X (2018) Punching holes on paper-like electrodes: an effective strategy to enhance rate performance of supercapacitors. *Energy Storage Mater.* <https://doi.org/10.1016/j.ensm.2018.10.008>
- Salari M, Konstantinov K, Liu H (2011) Enhancement of the capacitance in TiO_2 nanotubes through controlled introduction of oxygen vacancies. *J Mater Chem* 21:5128–5133

Publisher’s Note Springer Nature remains neutral with regard to jurisdictional claims in published maps and institutional affiliations.